

Pseudopolar smectic-*C* phases of azo-substituted achiral bent-core hockey-stick-shaped moleculesDeepshika Malkar,¹ M. Monika,² Veena Prasad,² and Arun Roy^{1,*}¹*Raman Research Institute, C. V. Raman Avenue, Sadashivanagar, Bangalore 560080, India*²*Centre For Nano and Soft Matter Sciences, Bangalore 560013, India*

(Received 20 June 2019; revised manuscript received 5 September 2019; published 2 January 2020)

We report experimental studies on an azo-substituted compound consisting of bent-core hockey-stick-shaped molecules. The experimental results establish two pseudopolar tilted smectic phases, which are characterized by an in-plane axial-vector order parameter in addition to tilt order in the smectic layers. Electro-optical measurements in the mesophases indicate that the birefringence of the sample strongly depends on the applied electric field. We develop a theoretical model to account for this observation. The change in the birefringence of the sample arises from the field-induced reorientation of the tilt plane of the molecules in the layer above a threshold field. The effect is analogous to the field-induced Freedericksz transition which is quadratic in the applied electric field.

DOI: [10.1103/PhysRevE.101.012701](https://doi.org/10.1103/PhysRevE.101.012701)**I. INTRODUCTION**

The realization of new thermodynamically stable liquid crystalline (LC) phases of compounds consisting of molecules of different shapes is an ongoing field of research [1–3]. The manifestation of polar order and spontaneous breaking of the chiral symmetry of achiral bent-core (BC) banana-shaped molecules in their tilted smectic phases led to considerable efforts to explore various phases of bent-core liquid crystals (BCLCs) [4,5]. However, most of the studies are performed on samples consisting of symmetric BC banana-shaped molecules. A typical BC banana-shaped molecule is made of two rigid rodlike arms of equal lengths joined end to end at an angle of about 120°. The bent configuration of the rigid arms gives rise to a shape polarity of the molecules, which accounts for many unusual properties of BCLCs [6,7]. A bent-core hockey-stick-shaped (BCHS) molecule is formed when one of the arms is relatively shorter than the other arm of the BC molecule. Thus the BCHS molecules have an intermediate shape between rodlike and BC banana-shaped molecules [8,9].

In the calamitic smectic-*C* (Sm*C*) phase exhibited by rodlike molecules, the molecules arrange themselves in fluid layers in which the long axes of the molecules are on average aligned at an angle with respect to the layer normal. It is experimentally found that within the layers, the molecules are almost freely rotating about their long axis, giving rise to an almost uniaxial local symmetry about the director [10]. On the other hand, for BC banana-shaped molecules in their tilted smectic phases, the free rotations of the molecules about their long axes are highly hindered due to the strong shape nonlinearity of the molecules. This effect gives rise to the polar order and consequent chiral symmetry breaking in the layers [11]. The polar order also gives rise to spontaneous electric polarization in the layers [6].

It is interesting to investigate the molecular organization of BCHS molecules in their tilted smectic phases as they have an intermediate shape between rodlike and BC banana-shaped molecules. Though there are some reports on hockey-stick-shaped molecules consisting of a rigid rodlike core with one of the terminal alkyl chains attached at an angle, i.e., at a meta position of the terminal phenyl ring to introduce the bent structure in the molecule [12–15], only a few studies have been carried out on the tilted smectic phases of BCHS molecules [16–21].

In our previous paper, we have reported the observation of two Sm*C* phases exhibited by a compound consisting of BCHS molecules [22]. We characterized these as pseudopolar Sm*C* phases because the molecules are tilted at an angle to the layer normal and the layers possess an in-plane axial-vector order parameter in addition to the tilt order. Here, in strong analogy with polar order in BC banana-shaped molecules, we denote the layers as pseudopolar even though there is no spontaneous electric polarization. In these phases, the BCHS molecules adopt a zigzag configuration for close packing in the layers. The molecules in the smectic layers align with a head-tail symmetry, and the average orientation direction of the long axes of the BCHS molecules, i.e., the director \hat{n} in a given layer, is at an angle with respect to the layer normal. In addition, the bend planes of zigzag molecules in a layer align on average parallel to the tilt plane, which induces an in-plane axial-vector order parameter in the layers. The layers in these smectic phases have an achiral C_{2h} point symmetry and do not possess any spontaneous electric polarization, hence the name pseudopolar. This is shown in Fig. 1, where $\vec{\xi}$ and $\vec{\eta}$ are the tilt and axial-vector order parameters in the plane of the layer. Figure 1(c) depicts the possible stacking of the layers in different phases. The lower-temperature Sm*C*₁ phase is characterized as a tilted smectic phase with the coexistence of degenerate structures of Sm*C*_α, Sm*C*₂, and Sm*C*_R, as discussed in our previous paper [22].

In this article, we report experimental studies of an azo-substituted compound consisting of BCHS molecules

*aroy@rri.res.in

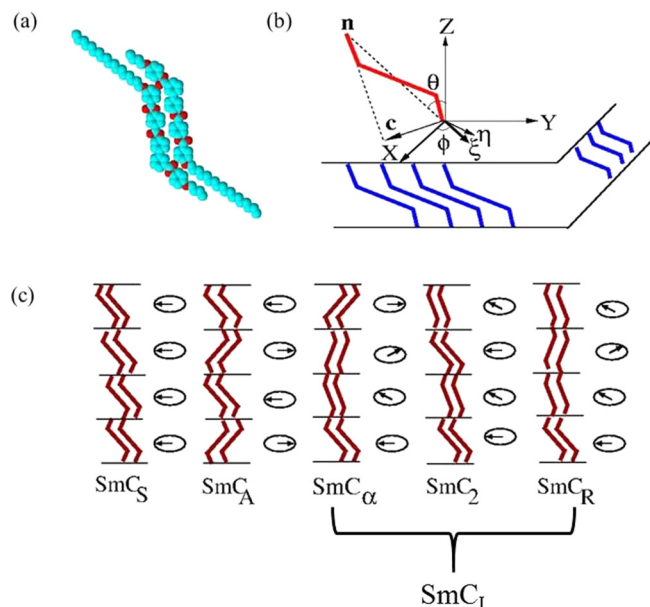


FIG. 1. (a) The zigzag configuration of the molecules in the layer. (b) The schematic representation of the order parameters in a given layer. (c) The possible layer stacking of the zigzag molecules in different tilted smectic phases (from Ref. [22]).

exhibiting similar tilted smectic phases. We also develop a theoretical model to describe the effect of an external electric field on the structure of these phases, which accounts for the observed electro-optic properties of the samples.

II. EXPERIMENTAL RESULTS

A. Sample and calorimetric studies

The molecular structure of the compound 4-(((3-((4-(n-Decyloxy)benzoyl)oxy)phenyl)imino)methyl)phenyl)-4-(4-(n-tetradecyloxy)phenyl)diazenyl)benzoate (A14) is shown in Fig. 2(a). The chemical synthesis and preliminary studies on this series of LC compounds have already been reported [23]. This molecule contains an azo-linkage group which shows light-induced isomerization when dissolved in a suitable solution [23]. However, we did not find any evidence of isomerization in their mesophases in visible light in the neat material. The differential scanning calorimetry (DSC) thermogram for compound A14 on heating and cooling is shown in Fig. 2(b). The DSC thermograms detect two mesophases between the isotropic liquid and crystal phases on cooling and heating at a rate of 3 K/min. The inset shows the weak first-order transition peaks between the observed mesophases. We designate the high- and low-temperature mesophases as SmC_A and SmC_I phases, respectively. The subscript *A* denotes the anticlinic arrangement of molecules in successive layers. The subscript *I* for the lower-temperature phase denotes an intermediate arrangement of molecules in successive layers with the azimuthal angle difference in tilt directions between 0 and π . This intermediate azimuthal angle difference in tilt directions is also observed in some ferroelectric phases exhibited by some rodlike chiral molecules [24–27]. However, it should be noted here that the layers in the observed SmC_A and SmC_I phases have

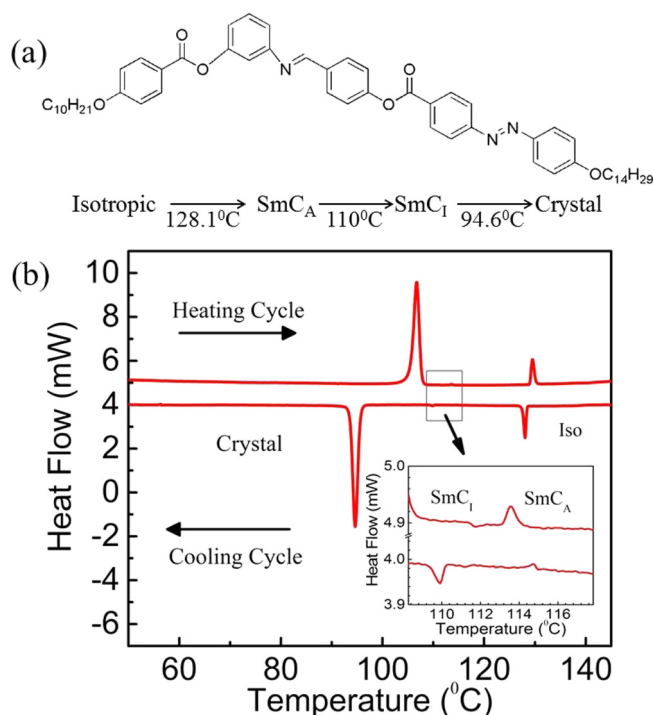


FIG. 2. (a) The molecular structure of the compound A14 and the phase sequence observed on cooling the sample from the isotropic phase. (b) The DSC thermogram on heating and cooling the sample at a rate of 3 K/min showing the transition peaks. The inset shows the weak first-order transition peak between the observed SmC phases.

no net electric polarization and are achiral in nature. The transition from the SmC_A to SmC_I phase is associated with a small change in enthalpy (0.11 kJ/mol), indicating a weak first-order phase transition. The phase sequence observed for this compound is similar to the phase behavior of a compound reported in our previous paper [22]. For a homeotropic alignment, the sample of thickness about 9 μm was sandwiched between a clean glass slide and a glass cover slip. For planar alignment, commercially available liquid crystal cells (INSTEC Inc.) of thickness 5 μm were used. The LC sample was introduced into liquid crystal cells by capillary action in the isotropic phase on a hot stage.

B. X-ray diffraction studies

The x-ray diffraction (XRD) studies were carried out on unoriented samples filled in Lindemann capillary tubes (outer diameter about 1 mm) while cooling the sample from the isotropic phase. The XRD intensity profile as a function of wave vector is shown in Fig. 3. In both mesophases, a sharp intense peak is observed at a small-angle range in addition to a diffusive wide-angle peak characteristic of the fluid lamellar smectic phase. The peak position at a small angle gives the effective layer spacing as 44.3 and 46.1 \AA in the SmC_A and SmC_I phases, respectively. The observed layer spacing in both phases is smaller than the molecular length (about 53 \AA) estimated from the molecular formula, indicating that the molecules are tilted with respect to the layer normal. Figure 4 shows the variation of layer spacing and tilt angle with temperature in both the SmC_A and SmC_I

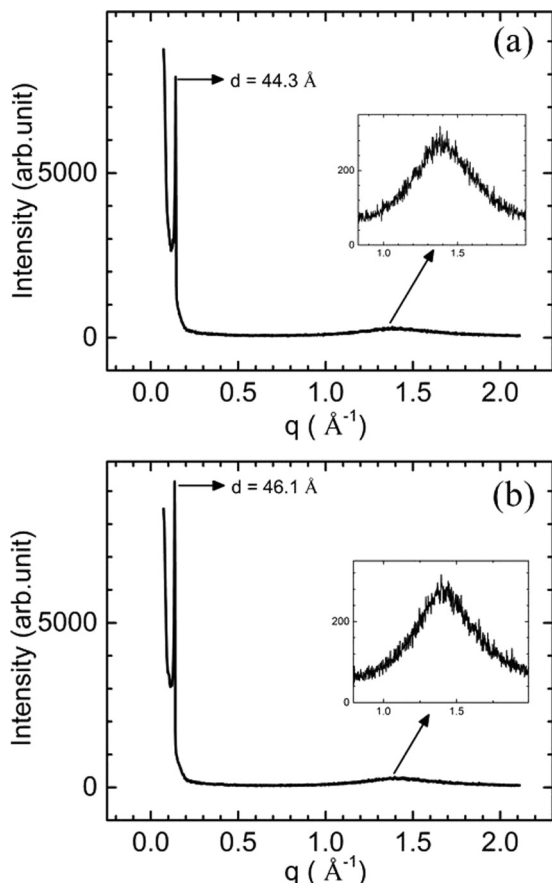


FIG. 3. The x-ray diffraction intensity profile in (a) SmC_A phase with layer spacing 44.3 \AA at 125°C and (b) SmC_I phase with layer spacing 46.1 \AA at 106°C . The insets show the enlarged view of the wide-angle peak.

phases. The tilt angle is calculated from the observed layer spacing assuming a constant molecular length using the formula $\theta = \cos^{-1}(d/l)$, where l is the molecular length and d is the measured layer spacing. The layer spacing (tilt angle) slightly increases (decreases) with decreasing the temperature in the SmC_A phase with a small jump at the SmC_A to SmC_I transition. The layer spacing (tilt angle) again slowly increases (decreases) on decreasing temperature within the SmC_I phase. The increment in the layer spacing is only about 4% over the whole temperature range studied. This can be attributed to a slight increase in the molecular length due to the stretching of terminal alkyl chains of the molecules with decreasing temperature.

C. Polarizing optical microscopy investigations

Polarizing optical microscopy (POM) studies were carried out for both planar and homeotropic alignment of the sample as shown in Fig. 5. For a homeotropically aligned sample, just below the transition temperature from the isotropic to the SmC_A phase, a birefringent schlieren texture is observed with the existence of half- and unit-strength defects [see Fig. 5(a)]. The appearance of a schlieren texture confirms the tilted nature of the molecules in the smectic layers as found in XRD studies. The presence of half-strength defects in the schlieren

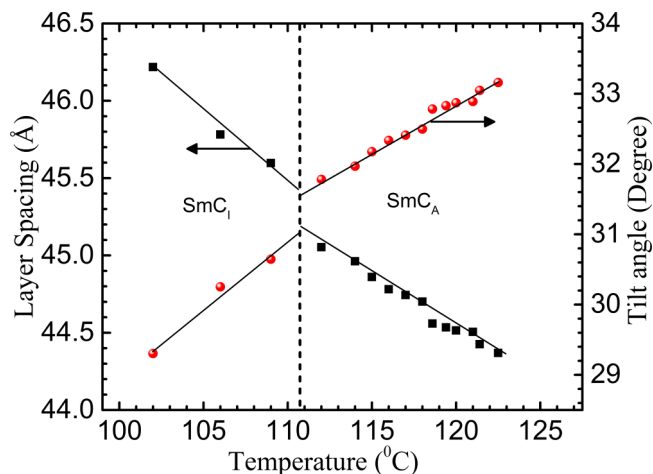


FIG. 4. The variation of the layer spacing and the calculated tilt angle as a function of temperature. The dashed line indicates the transition temperature between the observed smectic phases and the solid lines through the data points are a guide to the eye.

texture indicates the anticlinic arrangement of molecules in successive layers in the higher-temperature SmC_A phase. The half-strength defects can arise from dispiration lines in the anticlinic SmC phase [28,29]. At lower temperatures in the SmC_A phase, the schlieren texture acquires birefringence colors [Fig. 5(b)] due to an increase in the birefringence of the sample. On further cooling, the sample goes to the lower-temperature SmC_I phase. Here again, a birefringent schlieren texture [Fig. 5(c)] is observed for the homeotropically aligned sample with the existence of some domain structures separated by walls. The presence of domains indicates the coexistence of different degenerate structures in this phase. For a planar-aligned sample, batonnet growth of the SmC_A phase is observed on cooling the sample from the isotropic phase at a rate of 1 K/min , as shown in Fig. 5(d). On further cooling of the sample, batonnet growth gives rise to a focal conic fan texture [Fig. 5(e)]. The extinction brushes in the focal conic fan texture appear parallel to the layer normal when it is parallel and perpendicular to the polarizer, indicating that one of the optic axes is parallel to the layer normal, as expected in the anticlinic SmC_A phase. A transition from the SmC_A to SmC_I phase takes place at around 110°C . In the SmC_I phase, a large number of irregular bands appear parallel to the layers [see Fig. 5(f)]. The presence of irregular bands renders the focal conic fans less visible, indicating the existence of different stable degenerate states in the SmC_I phase.

We also measured the change in the average transmitted intensity of the POM images of the planar-aligned sample between crossed polarizers as a function of temperature. To calculate the average transmitted intensity, the POM images have been taken at a constant interval of temperature using a red filter. The red average transmitted intensity has been extracted from POM images by averaging over the pixels using a MATLAB program. The variation of the average transmitted intensity as a function of temperature on cooling the sample from the isotropic phase is shown in Fig. 6. The transition between different phases can be clearly detected from the variation of average transmitted intensity with decreasing

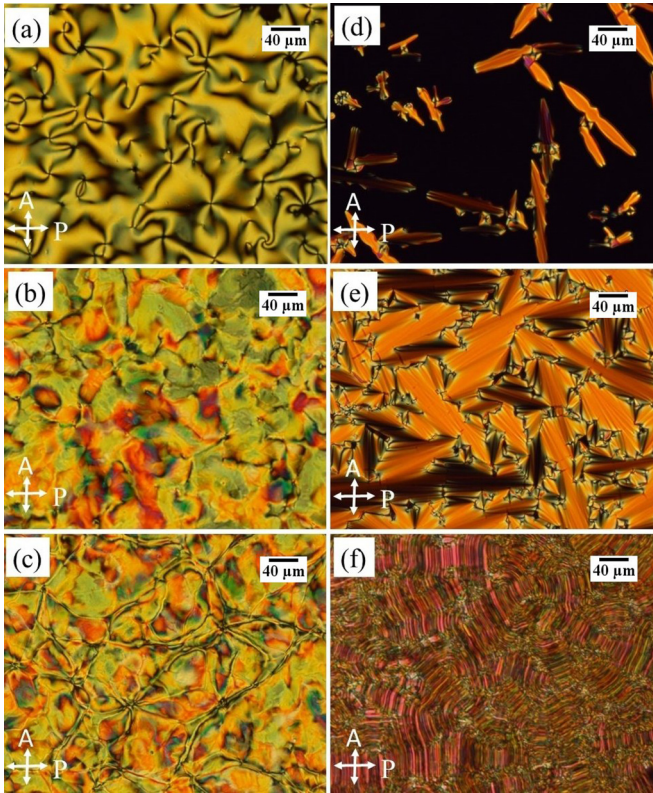


FIG. 5. Polarizing optical microscopy textures (left column) for a homeotropically aligned sample: (a) Schlieren texture with the unit- and half-strength defects just below the clearing temperature in the SmC_A phase, (b) at a lower temperature in the SmC_A phase, and (c) in the SmC_I phase. Right: For a planar-aligned sample, (d) the smectic batonnet growth just below the clearing temperature in the SmC_A phase, (e) completely grown focal conic fan texture in the SmC_A phase, and (f) irregular band texture in the SmC_I phase. The scale bar in the above images is $40 \mu m$.

temperature. At the transition from the isotropic to SmC_A phase, the intensity increases sharply due to the increase in birefringence of the sample below the transition point which saturates at lower temperatures in the SmC_A phase. At

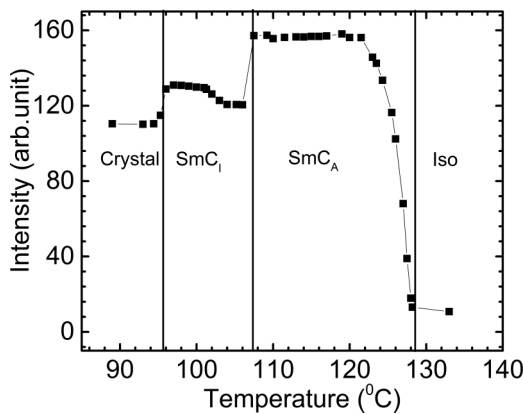


FIG. 6. The variation of average transmitted intensity of POM images with temperature of a planar-aligned sample of thickness $5 \mu m$ between crossed polarizers.

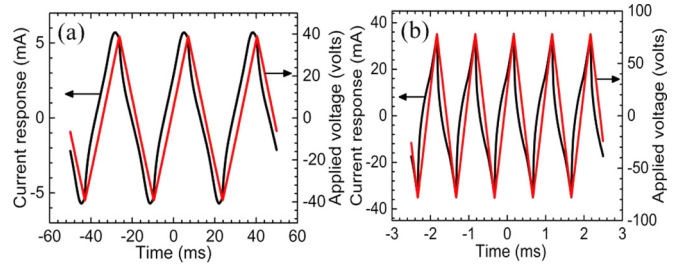


FIG. 7. The current response of compound A14 under the application of triangular wave voltage in the (a) SmC_A phase ($40 V, 30 Hz$) at $120^\circ C$ and (b) SmC_I phase ($80 V, 1 kHz$) at $102^\circ C$.

the transition point from the SmC_A to SmC_I phase, a sharp decrease in the intensity was observed due to the growth of irregular bands in the texture of the SmC_I phase.

D. Polarization switching current measurements

The polarization state of the layers in both the smectic phases can be determined by the electric current response of a planar-aligned sample under the application of a triangular wave voltage [30]. At a given temperature, the current response is determined by measuring the voltage drop across a $1 k\Omega$ resistor connected in series with the sample. For these measurements, a commercial liquid crystal cell of thickness $5 \mu m$ with the glass plates treated for planar alignment of the molecules was used. The sample was slowly cooled from the isotropic phase to the SmC_A phase in the presence of a low-frequency electric field ($\sim 3 V/\mu m, 10 Hz$) in order to induce planar alignment. The current response in the SmC_A phase is shown in Fig. 7(a). The conductive and dielectric currents mostly contribute to the current response in our sample. If the sample have ferro- or antiferroelectric properties, one or two additional polarization reversal current peaks are expected in one half cycle of the current response, respectively. The absence of polarization reversal current peaks indicates the lack of net electric polarization in the smectic layers in the SmC_A phase. The observed current response in the lower-temperature SmC_I phase is shown in Fig. 7(b). The current response is similar to that in SmC_A phase as the conductive and dielectric contributions to current response do not change significantly across the phase transition. Again, the absence of polarization reversal current peaks in the current response confirms the lack of layer polarization in the SmC_I phase. Therefore, we concluded from this experiment that the layers in both phases do not possess net electric polarization.

E. Steady-state electro-optical response

An optical response of the sample between crossed polarizers was observed upon application of an AC voltage, even in the absence of net electric polarization in the layers. The time-dependent electro-optic response of the sample while held at a constant temperature was characterized by measuring the transmitted intensity of a He-Ne laser passing through the planar-aligned sample of thickness $5 \mu m$ between crossed polarizers. The transmitted intensity was monitored using a high-gain, low-noise photodiode. The output signal of the photodiode was measured by an oscilloscope (Agilent

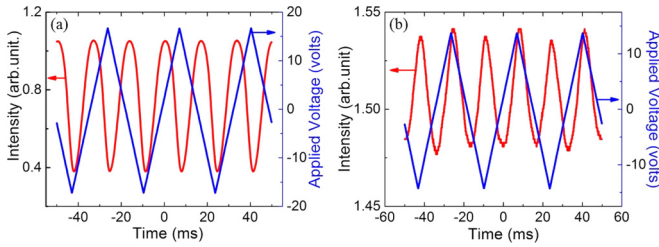


FIG. 8. Optical response of a planar-aligned sample of thickness $5 \mu\text{m}$ under the application of a triangular wave voltage in the (a) SmC_A and (b) SmC_I phases.

Technologies MSO6012A). The steady-state electro-optic response in both the SmC_A and SmC_I phases under the application of a triangular wave voltage of frequency 30 Hz is shown in Fig. 8. It should be noted that the transmitted intensity decreases (increases) with an increasing field in the SmC_A (SmC_I) phases, respectively. This is due to the zero-field optical phase difference ($\Delta\Phi_0$) introduced by the sample between the ordinary and extraordinary rays. For the studied sample in the SmC_A phase, $\Delta\Phi_0$ lies between π and 2π . The optical phase difference ($\Delta\Phi$) increases with applied field, giving rise to a decrease in transmitted intensity [see Eq. (1)] in the SmC_A phase, whereas in the lower-temperature SmC_I phase, due to the coexisting degenerate structures, $\Delta\Phi_0$ may lie between zero and π , giving rise to an increasing intensity with increasing field. The observed electro-optic response is symmetric with respect to the positive and negative value of the applied voltage, indicating a quadratic coupling of the electric field with the effective dielectric anisotropy of the sample. The electro-optic response clearly originates from the effective change in the birefringence of the sample due to the reorientation of the molecules in the smectic layers under applied fields. The measured optical contrast is smaller in the lower-temperature SmC_I phase compared to that in the SmC_A phase due to the coexistence of bands in the texture of the SmC_I phase.

F. Dielectric constant measurements

The real part of the effective dielectric constant of a planar-aligned sample of thickness $5 \mu\text{m}$ was measured as a function of temperature on cooling from the isotropic phase. Briefly, a sinusoidal AC voltage of frequency 5641 Hz and amplitude 0.5 V was applied to a series circuit of the sample and 1 k Ω resistor. The voltage across the resistor was measured using a lock-in amplifier (SRS830). The temperature was controlled to $\pm 0.1^\circ\text{C}$ by an INSTRON controller and the whole apparatus was controlled by a customized LabVIEW program. Using impedance analysis, we determined the capacitance of the sample from which the effective dielectric constant was extracted by taking the ratio to the empty cell capacitance measured prior to filling the sample in the liquid crystal cell. Figure 9 shows the temperature variation of the real part of the effective real dielectric constant on cooling from the isotropic phase. The measured dielectric constant increases on cooling from the isotropic phase and exhibits a slope discontinuity at the transition to the SmC_A phase. On further decreasing the temperature, the dielectric

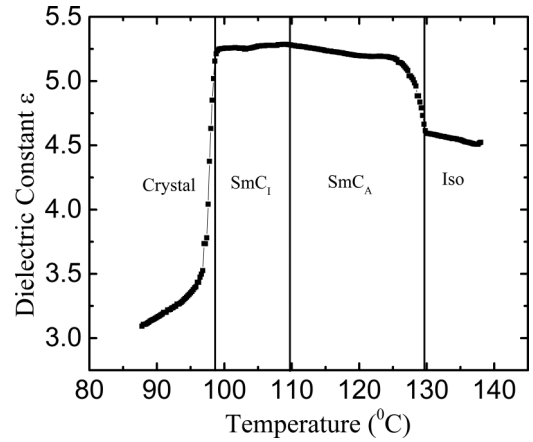


FIG. 9. The variation of the effective dielectric constant as a function of temperature for the planar-aligned sample of thickness $5 \mu\text{m}$.

constant saturates to a value of approximately 5.25, and it varies continuously across the SmC_A to the SmC_I phase. The low value of the dielectric constant in both the smectic phases again confirms the absence of polarization in the layers. Assuming that the component of the dielectric tensor perpendicular to the director (ϵ_{\perp}) mostly contributes to the measured dielectric constant of the planar aligned sample in the smectic phases, the higher value of the measured dielectric constant in the smectic phases compared to that in the isotropic phase indicates negative dielectric anisotropic behavior of the sample [31].

G. Electric field effects on POM textures

To further investigate the structures of both of the mesophases, we measured field-induced changes in the birefringence of a planar-aligned sample of thickness $5 \mu\text{m}$. The sample was slowly cooled from the isotropic to the SmC_A phase and observed between crossed polarizers in a polarizing optical microscope (Olympus BX-50). A focal conic fan texture [Fig. 10(a)] was observed in the SmC_A phase in the absence of an applied electric field. The changes in the birefringence color of the sample in the SmC_A phase with increasing an applied AC electric field is shown in Fig. 10. Interestingly, it was found that upon increasing the applied electric field, the birefringence color starts to change above a threshold field ($\sim 4 \text{ V}/\mu\text{m}$). On further increasing applied field, the birefringence color changes gradually from purple to blue [Figs. 10(b) and 10(c)]. At even higher field, the birefringence color changes to green [Fig. 10(d)] and then it tends to saturate. The changes in the color of the sample without any rotation of the extinction brushes with increasing applied field imply an increase in birefringence with the local optic axis remaining the same. The birefringence color of the sample in the SmC_I phase also changes with increasing field (see Fig. 11). However, because of the random texture, the birefringence of the sample cannot be estimated in the SmC_I phase. The irregular bands in the SmC_I phase tend to decrease in number at high field, as can be seen in Fig. 11(d).

To quantitatively measure the effective birefringence of a planar-aligned sample in the SmC_A phase, we measured

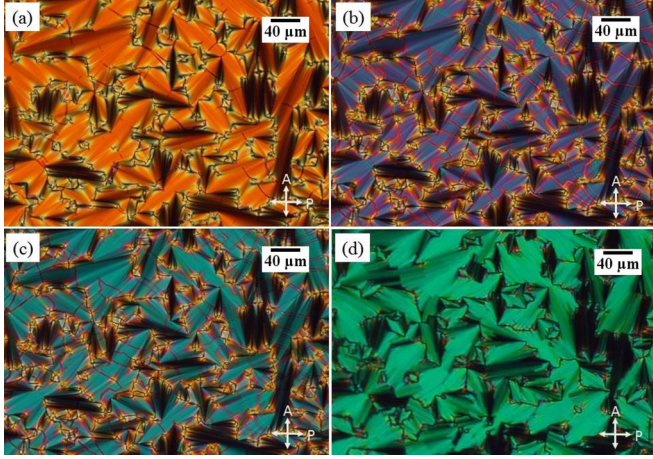


FIG. 10. The changes in the birefringence color of the sample at 115 °C in the SmC_A phase under the application of an AC electric field of frequency 1 kHz with increasing amplitudes: (a) 0 $V/\mu m$, (b) 4.4 $V/\mu m$, (c) 8.6 $V/\mu m$, and (d) 16 $V/\mu m$. The scale bar used in all the images is 40 μm .

the variation of average transmitted intensity of the sample with increasing amplitude of an applied AC electric field of frequency 1 kHz. To determine the average transmitted intensity, we have taken the images of a planar-aligned sample using a red filter under crossed polarizers at a constant temperature with a varying amplitude of the applied field. The red average transmitted intensity was extracted from POM images using a MATLAB program. The variation of average transmitted intensity with field in the SmC_A phase is shown in Fig. 12(a). As observed in POM investigations, the textural intensity remains nearly constant up to a threshold field ($\sim 4 V/\mu m$) above which the intensity starts to decrease gradually with increasing field. The gradual decrease in the intensity above the threshold field implies an increase in the effective birefringence in this case. We

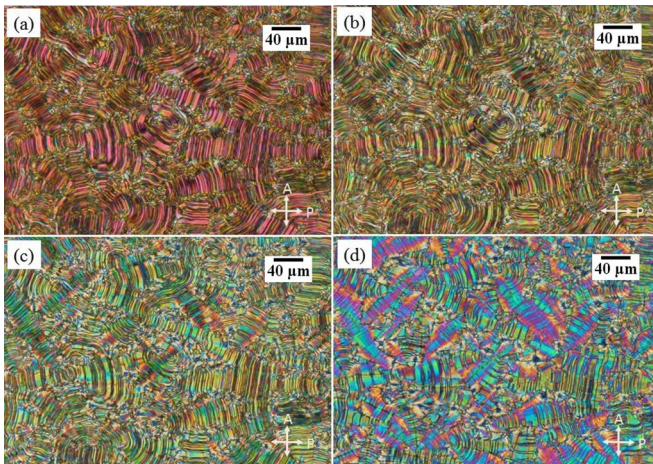


FIG. 11. The changes in the POM texture of a planar-aligned sample in the SmC_l phase under the application of an AC electric field of frequency 1 kHz with increasing amplitudes: (a) 0 $V/\mu m$, (b) 4.4 $V/\mu m$, (c) 8.6 $V/\mu m$, and (d) 16 $V/\mu m$ at 104 °C. The scale bar used in all the images is 40 μm .

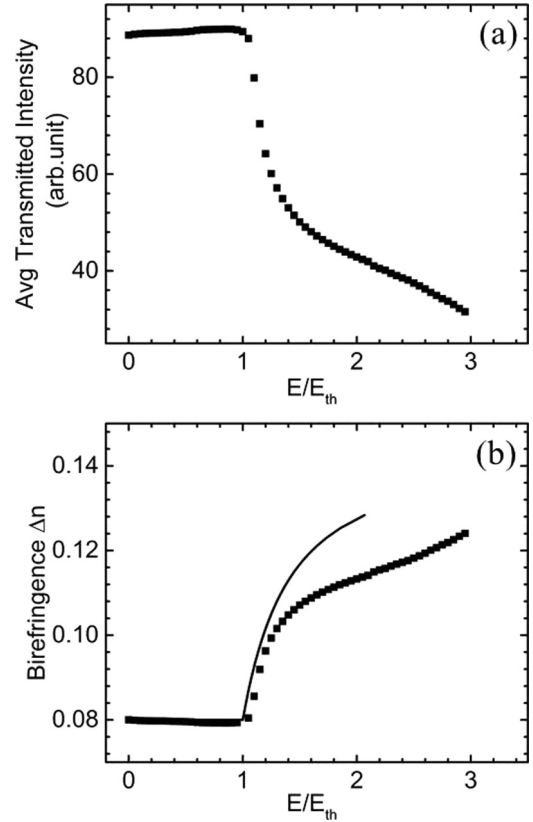


FIG. 12. (a) The variation of average transmitted intensity and (b) the effective birefringence of a planar-aligned sample in the SmC_A phase with increasing amplitude of the applied electric field of frequency 1 kHz. The data points are experimental values whereas the solid line shows the theoretically calculated value of the effective birefringence using our model.

estimated the change in the effective birefringence of the planar-aligned sample in the SmC_A phase with an applied field as follows:

The transmitted intensity at a given pixel of the POM image of the planar-aligned sample under an applied electric field can be written as

$$I = \frac{I_i}{2} \sin^2(2\psi)(1 - \cos \Delta\Phi), \quad (1)$$

where I_i is the incident intensity of light, ψ is the angle between local optic axis and the polarizer, and $\Delta\Phi = (2\pi \Delta n d)/\lambda$ is the local phase difference. Here, d is the sample thickness, and λ is the wavelength of the incident light. In our experiments, we have used a red filter of wavelength $\lambda = 650$ nm. The Δn is the effective birefringence of the sample at that pixel under an applied field. As the angle ψ at a given pixel does not change under the application of the field, we can write

$$\sqrt{\frac{I}{I_0}} = \frac{\sin \frac{\Delta\Phi}{2}}{\sin \frac{\Delta\Phi_0}{2}}, \quad (2)$$

where the subscript 0 denotes the value of that quantity at zero electric fields. In our experiments, we estimate $\Delta n_0 = 0.080$ from the birefringence color in the focal conic fan texture of the SmC_A phase in the absence of electric field

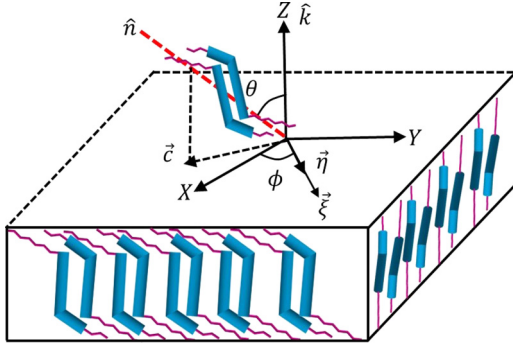


FIG. 13. The zigzag configuration of BCHS molecules in a layer of the observed smectic phases. The order parameters $\tilde{\xi}$, $\tilde{\eta}$, and \tilde{c} denote the tilt order, axial-vector order, and c director in the plane of the layer, respectively. Note that the order parameters $\tilde{\xi}$ and $\tilde{\eta}$ are parallel to each other.

using the Michel-Lévy interference color chart and we write $\Delta\Phi = \Delta\Phi_0 + \delta\Phi$, where $\delta\Phi$ is the small change in the phase difference in the presence of an applied electric field. Assuming the field-induced change in the phase difference $\delta\Phi$ is small, we can write

$$\delta\Phi = 2 \tan\left(\frac{\Delta\Phi_0}{2}\right) \left(\sqrt{\frac{I}{I_0}} - 1\right). \quad (3)$$

Using Eq. (3), we estimated the change in the effective birefringence of the sample in the SmC_A phase at each pixel and the mean value of the birefringence is obtained by averaging over the pixels of the POM image. The changes in the effective birefringence of the planar-aligned sample in the SmC_A phase with the field is shown in Fig. 12(b). The effective birefringence increases with increasing field above the threshold value.

III. THEORETICAL MODEL FOR FIELD-INDUCED CHANGES IN BIREFRINGENCE

We now describe a theoretical model to account for the electric-field-induced change in the effective birefringence of a planar-aligned sample in the SmC_A phase, in particular, the threshold field effect observed experimentally in our system. A simple theoretical model to account for the observed phases has been described in our previous paper [22]. In the SmC_A phase, the tilt order of the BCHS molecules in a layer can be described by an axial vector, $\tilde{\xi} = (\hat{k} \cdot \hat{n})(\hat{k} \times \hat{n})$, where the unit vectors \hat{k} and \hat{n} denote the layer normal and average orientation direction of the long axes of the molecules, respectively [32,33]. The c director \tilde{c} is defined as the projector of director \hat{n} onto the layer plane which is perpendicular to $\tilde{\xi}$. The rigid bent ends of the BCHS molecules strongly hinder the free rotation of the molecules about their long axis in the tilted smectic layers. Therefore the packing and entropy considerations favor a zigzag configuration of the BCHS molecules in the tilted smectic layers [22,34]. When the long axes of these zigzag molecules are on average tilted, the tilt plane favors the bend plane of the zigzag molecules aligned parallel to itself (see Fig. 13). This orientational order of the short axis of the BCHS molecules can be described

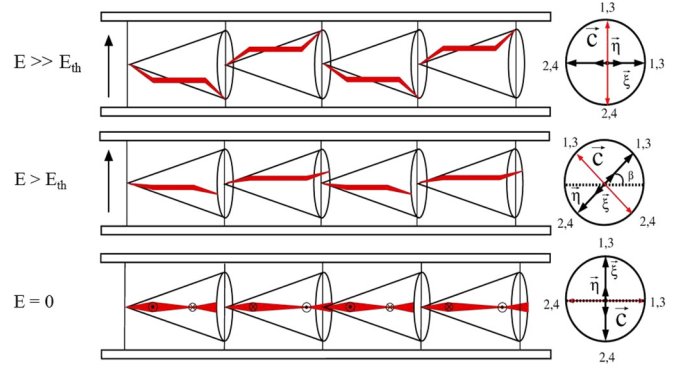


FIG. 14. The schematic representation of the molecular organization at the midplane of the cell in the smectic layers in a bookshelf geometry between two glass plates at different electric fields. The circles on the right side represent the orientation of the vectors $\tilde{\xi}$, $\tilde{\eta}$, and \tilde{c} (red arrow) in smectic layers viewed along the layer normal. The numbers 1,2,3, ... represent the corresponding sequence of the layers.

by an axial-vector order parameter $\tilde{\eta}$. The order parameters $\tilde{\xi}$ and $\tilde{\eta}$ have the same symmetry and the lowest-order bilinear coupling favors them to be parallel to each other [22]. These types of the ordering of BCHS molecules render the smectic layers strongly biaxial with three principle dielectric constants $\epsilon_3 < \epsilon_1 < \epsilon_2$, where ϵ_3 and ϵ_1 denote the principle dielectric constant parallel to the director and perpendicular to the tilt plane, respectively. The dielectric component ϵ_2 corresponds to the principle component in the tilt plane of the molecules in a layer. Assuming a bookshelf geometry of the layers in the SmC_A phase between the glass plates of the liquid crystal cell, both the tilt order $\tilde{\xi}$ and the axial-vector order $\tilde{\eta}$ are perpendicular to the bounding glass plates in the absence of field (Fig. 14, bottom). Thus the dielectric tensor in the SmC_A phase can be written by averaging over adjacent layers as

$$\epsilon_{ij} = \begin{pmatrix} \epsilon_2 \cos^2 \theta + \epsilon_3 \sin^2 \theta & 0 & 0 \\ 0 & \epsilon_1 & 0 \\ 0 & 0 & \epsilon_2 \sin^2 \theta + \epsilon_3 \cos^2 \theta \end{pmatrix}.$$

Here, we have assumed the z axis along with the layer normal, the y axis is normal to the glass plates of the cell, and the x axis is in the plane of the glass plates orthogonal to both the z and y axis and θ is the tilt angle.

However, in the presence of the applied field along the y axis, the field tends to align the tilt plane of the molecules due to the dielectric anisotropy of the layers, whereas the strong anchoring on the glass plates tends to retain the tilt plane of the molecules parallel to themselves. Above a threshold field, the tilt plane of the molecules makes an angle β with the horizontal xz plane while retaining anticlinic organization in the SmC_A phase (Fig. 14, middle). The angle β at the midplane of the cell (β_m) tends to the value of $\pi/2$ at a very high field (Fig. 14, top). The free-energy density per unit area of the sample cell can be written as

$$f = \frac{1}{2} K \left(\frac{d\beta}{dy}\right)^2 - \frac{1}{2} \epsilon_0 E^2 [\tilde{\Delta}\epsilon \sin^2 \beta + \epsilon_1]. \quad (4)$$

Here, K is a suitable elastic constant corresponding to the distortion of the angle β across the sample cell and the last term corresponds to the free-energy density in the presence of the electric field. The $\widetilde{\Delta\epsilon}$ is the effective dielectric anisotropy of the sample in this configuration. The $\widetilde{\Delta\epsilon}$ is given by

$$\widetilde{\Delta\epsilon} = \delta\epsilon \cos^2 \theta + \Delta\epsilon \sin^2 \theta, \quad (5)$$

where $\Delta\epsilon = (\epsilon_3 - \epsilon_1)$ and $\delta\epsilon = (\epsilon_2 - \epsilon_1)$ are the dielectric anisotropy and dielectric biaxiality of the sample in the SmC_A phase.

The free-energy density in Eq. (4) is analogous to that of a planar-aligned nematic sample under an electric field [35] and predicts a Fredericksz-type transition above a threshold field for $\widetilde{\Delta\epsilon} > 0$. The threshold field is given by

$$E_{\text{th}} = \frac{\pi}{d} \sqrt{\frac{K}{\epsilon_0 \widetilde{\Delta\epsilon}}}. \quad (6)$$

Assuming the elastic constant $K \sim 10^{-10}$ N in the SmC_A phase and $\widetilde{\Delta\epsilon} \sim 0.2$, the calculated threshold field from Eq. (6) is quite close to the experimentally measured threshold field in the SmC_A phase.

We also calculate the β profile across the thickness of the sample cell. The minimization of free energy, $F = \int_0^d f dy$, gives a nonlinear Euler-Lagrange equation which has been solved using MATHEMATICA. We assume the strong anchoring condition $\beta = 0$ at both the bounding glass plates. Figure 15(a) shows the profile of β across the cell for different fields normalized with respect to the threshold field. The β profile depicts the reorientation of the tilt plane of the molecules above the threshold field keeping an anticlinic arrangement in successive layers. For a given field, β attains the maximum value β_m at the midplane of the cell, and its value increases with increasing field. Figure 15(b) shows the variation of β_m with increasing applied field. We also calculate the effective birefringence of the sample based on the calculated profile of β . For the calculation of effective birefringence, we assume the principle refractive indices of a layer as $n_3 = 1.7$, $n_2 = 1.5$, and $n_1 = 1.48$. For a given value of β , using the above principle refractive indices and the experimentally measured tilt angle, we calculate the local birefringence in the anticlinic SmC_A phase. The effective birefringence of the sample cell is then calculated by integrating over the cell thickness. For a comparison with the experimental data, the calculated effective birefringence as a function of an applied field is shown in Fig. 12(b). The model accounts for the observed threshold behavior in the changes of the birefringence of the sample with field in the higher-temperature SmC_A phase. The theoretical values compare well with the experimental data near the threshold field, though they deviate significantly at higher fields. In the model, we have assumed the perfect alignment of the sample with the bookshelf geometry of the layers. However, in the experimental liquid crystal cell, the alignment is far from perfect, and there are multiple domains with defects in the texture. The deviations between the experimental and theoretical values possibly arise because of the presence of these defects in the texture. The onset of electrohydrodynamic instability at high

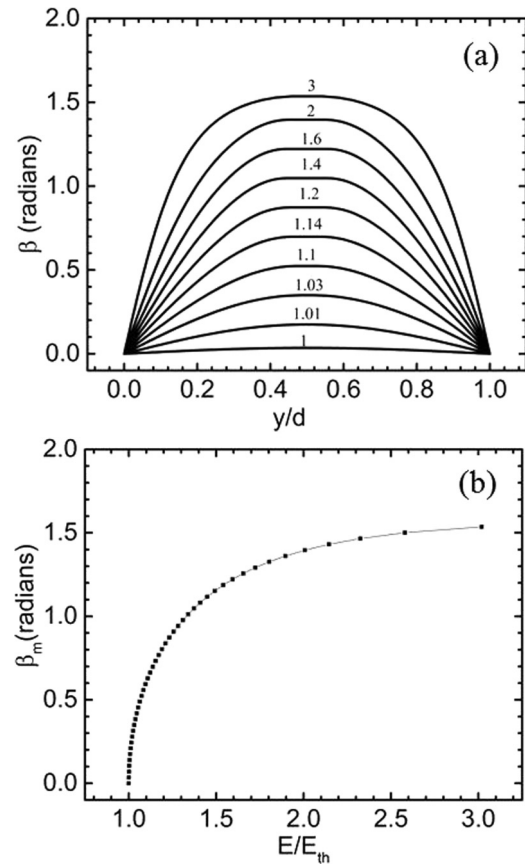


FIG. 15. (a) The variation of tilt plane angle β across the sample cell at different normalized electric fields. (b) The variation of the maximum value of β at the midplane (β_m) as a function of the normalized electric field $\frac{E}{E_{\text{th}}}$.

fields (above $10 \text{ V}/\mu\text{m}$) also leads to further complications in the measurements of the birefringence of the sample. The existence of the Fredericksz transition in the SmC phase has been reported [36] earlier for a sample consisting of rodlike molecules with positive dielectric anisotropy. However, as can be seen from Eq. (5), the effective dielectric anisotropy $\widetilde{\Delta\epsilon}$ can be positive for our sample even with $\Delta\epsilon < 0$ but $\delta\epsilon > 0$. The Fredericksz-type transition has also been observed in surface-stabilized antiferroelectric liquid crystals consisting of chiral molecules [37].

In conclusion, we have performed detailed experimental studies on two tilted smectic phases consisting of bent-core hockey-stick-shaped molecules. The experimental results indicate that these tilted smectic phases are characterized by an in-plane axial-vector order in addition to the tilt order in the layers. We also develop a simple model to account for the observed electro-optic effects in the sample. We predict a Fredericksz-type transition in the SmC_A phase above a threshold field.

ACKNOWLEDGMENT

We thank Vashudha K. N. for technical assistance in taking the XRD and DSC data.

- [1] S. Chandrasekhar, *Liquid Crystals* (Cambridge University Press, Cambridge, UK, 1992).
- [2] H. Takezoe and L. Eremín, *Bent-Shaped Liquid Crystals: Structures and Physical Properties* (CRC Press, Boca Raton, FL, 2017).
- [3] A. Jakli and A. Saupe, *One- and Two-Dimensional Fluids: Physical Properties of Smectic, Lamellar, and Columnar Liquid Crystals* (CRC Press, Boca Raton, FL, 2006).
- [4] T. Niori, T. Sekine, J. Watanabe, T. Furukawa, and H. Takezoe, *J. Mater. Chem.* **6**, 1231 (1996).
- [5] J. W. Goodby, P. J. Collings, T. Kato, C. Tschierske, H. F. Gleeson, and P. Raynes, *Handbook of Liquid Crystals*, 2nd ed. (Wiley-VCH, Weinheim, 2014), Vol. 4.
- [6] R. A. Reddy and C. Tschierske, *J. Mater. Chem.* **16**, 907 (2006).
- [7] F. C. Yu and L. J. Yu, *Chem. Mater.* **18**, 5410 (2006).
- [8] T. J. Dingemans, N. S. Murthy, and E. T. Samulski, *J. Phys. Chem. B* **105**, 8845 (2001).
- [9] M. Horcic, V. Kozmik, J. Svoboda, and V. Novotna, *J. Mater. Chem. C* **1**, 7560 (2013).
- [10] Z. Luz and S. Meiboom, *J. Chem. Phys.* **59**, 275 (1973).
- [11] D. R. Link, G. Natale, R. Shao, J. E. MacLennan, N. A. Clark, E. Korblova, and D. M. Walba, *Science* **278**, 1924 (1997).
- [12] F. C. Yu and L. J. Yu, *Liq. Cryst.* **35**, 799 (2008).
- [13] B. Das, S. Grande, W. Weissflog, A. Eremín, M. W. Schröder, G. Pelzl, S. Diele, and H. Kresse, *Liq. Cryst.* **30**, 529 (2003).
- [14] A. Chakraborty, M. K. Das, B. Das, U. Baumeister, and W. Weissflog, *J. Mater. Chem. C* **1**, 7418 (2013).
- [15] R. Stannarius, J. Li, and W. Weissflog, *Phys. Rev. Lett.* **90**, 025502 (2003).
- [16] P. Sathyanarayana, S. Radhika, B. K. Sadashiva, and S. Dhara, *Soft Matter* **8**, 2322 (2012).
- [17] M. Alaasar, *Liq. Cryst.* **43**, 2208 (2016).
- [18] S. Radhika, H. T. Srinivasa, and B. K. Sadashiva, *Liq. Cryst.* **38**, 785 (2011).
- [19] M. Alaasar, S. Poppe, C. Kerzig, C. Klopp, A. Eremín, and C. Tschierske, *J. Mater. Chem. C* **5**, 8454 (2017).
- [20] D. D. Sarkar, R. Deb, N. Chakraborty, and V. S. R. Nandiraju, *Liq. Cryst.* **39**, 1003 (2012).
- [21] E. R. Cioanca, E. L. Epure, I. Carlescu, G. Lisa, D. Wilson, N. Hurduc, and D. Scutaru, *Mol. Cryst. Liq. Cryst.* **537**, 51 (2011).
- [22] D. Malkar, B. K. Sadashiva, and A. Roy, *Soft Matter* **12**, 4960 (2016).
- [23] M. Monika, Veena Prasad, and N. G. Nagaveni, *Liq. Cryst.* **42**, 1490 (2015).
- [24] A. Roy and N. V. Madhusudana, *Europhys. Lett.* **36**, 221 (1996).
- [25] P. M. Johnson, D. A. Olson, S. Pankratz, T. Nguyen, J. Goodby, M. Hird, and C. C. Huang, *Phys. Rev. Lett.* **84**, 4870 (2000).
- [26] L. S. Matkin *et al.*, *Phys. Rev. E* **64**, 021705 (2001).
- [27] I. Musevic and M. Skarbot, *Phys. Rev. E* **64**, 051706 (2001).
- [28] Y. Takanishi, H. Takezoe, A. Fukuda, H. Komura, and J. Watanabe, *J. Mater. Chem.* **2**, 71 (1992).
- [29] Y. Takanishi, H. Takezoe, A. Fukuda, and J. Watanabe, *Phys. Rev. B* **45**, 7684 (1992).
- [30] K. Miyasato, S. Abe, H. Takezoe, A. Fukuda, and E. Kuze, *Jpn. J. Appl. Phys.* **22**, L661 (1983).
- [31] W. H. de Jeu, *Physical Properties of Liquid Crystalline Materials* (Gordon and Breach, London, 1980).
- [32] A. Roy, N. V. Madhusudana, P. Toledano, and A. M. Figueiredo Neto, *Phys. Rev. Lett.* **82**, 1466 (1999).
- [33] V. L. Lorman, A. A. Bulbitch, and P. Toledano, *Phys. Rev. E* **49**, 1367 (1994).
- [34] E. N. Keller, E. Nachaliel, D. Davidov, and C. Böffel, *Phys. Rev. A* **34**, 4363 (1986).
- [35] P. G. de Gennes and J. Prost, *The Physics of Liquid Crystals* (Clarendon Press, Oxford, UK, 1994).
- [36] G. Pelzl, P. Kolbe, U. Preukschas, S. Diele, and D. Demus, *Mol. Cryst. Liq. Cryst.* **53**, 167 (1979).
- [37] B. Wen, S. Zhang, S. S. Keast, M. E. Neubert, P. L. Taylor, and C. Rosenblatt, *Phys. Rev. E* **62**, 8152 (2000).